HEFAT2014
10th International Conference on Heat Transfer, Fluid Mechanics and Thermodynamics
14 – 26 July 2014
Orlando, Florida

EFFECTS OF THERMAL BOUNDARY CONDITIONS ON NATURAL CONVECTION IN A SQUARE ENCLOSURE WITH AN INNER CIRCULAR CYLINDER DIFFERDENTIALLY HEATED FROM BOTTOM WALL

Minsung Kim[a], Jeong Hoon Doo[c], Man Yeong Ha[a]* and Hyun Sik Yoon[b]
a School of Mechanical Engineering, Pusan National University, San 30, Jangjeon-dong, Geumjeong-gu, Busan 609-735, Korea
b Global Core Research Center for Ships and Offshore Plants, Pusan National University, San 30, Jangjeon-dong, Geumjeong-gu, Busan 609-735, Korea
c Rolls-Royce PLC, Installations and Controls; P.O. BOX 31, Moor Lane, Derby DE24 8BJ, United Kingdom
E-mail: kms514v@pusan.ac.kr

ABSTRACT

Two-dimensional numerical simulations are carried out for natural convection in an enclosure with an hot inner cylinder located at the center for four different Rayleigh numbers of 10^3 , 10^4 , 10^5 and 10^6 . The immersed boundary method (IBM) was used to handle the virtual surface of the inner circular cylinder with a no-slip boundary condition. The Prandtl number *Pr* was taken to be 0.7 corresponding to that of air. This study focuses on the effect of the temperature variation of bottom wall of the enclosure on thermal and flow structures of natural convection. The results indicate negligible changes in thermal and flow structures based on variations in the size of the local heating zone on the bottom wall at $Ra = 10^3$ and 10^4, although there is a small variation in the convection velocity in the enclosure. At $Ra = 10^5$, small inner vortices formed in the lower part of the cylinder show significant changes in their size with increases due to increasing the bottom wall temperature. At $Ra = 10^6$, the magnitude of convection velocity becomes much larger than that when $Ra = 10^5$. As a result, much stronger rising plumes than those for $Ra = 10^5$ were formed on the top of the cylinder. And the secondary vortices form and separate above the bottom surface of the cylinder. The generation and dissolution of vortices are dependent mainly on the temperature of bottom wall in the enclosure.

INTRODUCTION

Natural convection phenomena are encountered in many practical applications such as the energy conservation in buildings, cooling of electronic equipment, cooling of nuclear reactor systems, solar engineering, and environmental and geothermal fluid dynamics. These application areas include the cooling of electronic devices, double-pane windows, heating and cooling of building, refrigerators, room ventilating, heat exchangers, solar collectors and so on.

NOMENCLATURE

Symbols

f_i	Momentum forcing
g	Gravitational acceleration
H	Vertical length of enclosure
L	Horizontal length of enclosure
n	Direction normal to the wall
Nu	Nusselt number
P	Pressure
Pr	Prandtl number
q	Mass source or sink
R	Radius of circular cylinder
Ra	Rayleigh number
t	Time
T	Temperature
u,v	Velocity components in x and y directions
x,y	Cartesian coordinates

Greek symbols

α	Thermal diffusivity
β	Thermal expansion coefficient
δ_{ij}	Kronecker delta
ρ	Density
ν	Kinematic viscosity
φ	Angle (degrees)
θ	Dimensionless temperature

Sub/superscripts

b	Bottom wall
c	Cold
cyl	Cylinder
h	Hot
t	Top
*	Dimensional variable

Mathematical symbols

$\langle\ \rangle$	Surface-averaged value

Due to a wide range of applications, fundamental studies on the natural convection in an enclosure, and Rayleigh-Bénard convection in a horizontal layer of the fluid confined between two parallel plates, have been performed by many investigators over the last few decades. Gelfgat [1] provided a complete numerical solution of a formulated benchmark problem devoted to the parametric study of Rayleigh-Bénard instability in rectangular two-dimensional (2-D) and three-dimensional (3-D) boxes. The results of the parametric calculations were presented in [1] as characteristic curves showing the dependence of the critical Rayleigh number on the aspect ratio of the cavity. Quertatani *et al.* [2] numerically performed a study on a classical Rayleigh-Bénard convection problem, and reported the characteristics of the flow and thermal structures for Rayleigh numbers ranging from 10^3 to 10^6. D'Orazio *et al.* [3] studied the case of 2-D Rayleigh-Bénard convection developed in a cavity with a large aspect ratio ranging between 2 and 6, where the Rayleigh number range of $10^3 \sim 2\times10^6$ was considered in the study.

In many engineering applications, the situation frequently arises wherein diverse thermal boundary conditions are imposed on walls of an enclosure. Therefore, many studies have considered the effect of a thermal boundary condition on natural convection. Corcione [4] studied natural convection in an air-filled rectangular enclosure heated from below and cooled from above with respect to variable thermal boundary conditions imposed on the side walls. The author reported that bi-direction differential heating has a significant effect on the flow mode transition of natural convection in the horizontal cavity. Kim *et al.* [5] recently investigated the natural convection induced by a temperature difference between a cold outer square cylinder and a hot inner cylinder for different Rayleigh numbers in the range of 10^3 to 10^6. The location of an inner circular cylinder was changed vertically along the centerline of the square enclosure. They reported that the numerical solutions for the flow and thermal fields eventually reach the steady state for all Rayleigh numbers considered. The number, size, and formation of the convection cells strongly depended on the Rayleigh number and the position of the inner circular cylinder. Kandaswamy *et al.* [6] numerically studied unsteady laminar natural convection in an enclosure with partially-heated side walls and an inner body as an internal heat source. They investigated the effects of the aspect ratio of the enclosure, different Prandtl numbers, and locations of the thermally active part of the side walls. They described the flow structure and the heat distribution in the enclosure, and the profile of the convection velocity in the mid-plane of the enclosure, for various simulation parameters. In addition, they assessed the heat transfer rate from walls of the enclosure. Aydin and Yang [7] numerically investigated the natural convection in a vertical square cavity with localized isothermal heating from below and symmetrical cooling from the side walls. They considered various length of the local heating zone as a main simulation parameter. They reported that the Nusselt number on the heated part of the bottom wall increases with increasing Rayleigh number and with the length of the heating zone. Basak *et al.* [8] studied the effects of thermal boundary conditions in a square enclosure on buoyancy-induced convection flow with respect to fluids with different Prandtl numbers by using the finite element method. They imposed a non-uniform heating condition on the bottom wall. They reported that the non-uniform heating of the bottom wall produces a greater heat transfer rate in the center region of the bottom wall than the rate produced in the uniform heating case for the Rayleigh numbers considered.

In our study, 2-D numerical simulations were performed for natural convection in a square enclosure with a hot inner circular cylinder for a wide range of Rayleigh numbers ($10^3 \le Ra \le 10^6$). We investigated the effect of various temperature conditions of the bottom wall on the characteristics of the flow structure and heat transfer of natural convection.

NUMERICAL METHODOLOGY

A schematic of the system is shown in Figure 1. The system consists of a square enclosure with sides of length L, within which a circular cylinder of radius R (= $0.2\,L$) is located at the center. As shown in Figure 1, the top and side walls of the enclosure are kept at a constant low temperature T_c, whereas the bottom wall of the enclosure is kept at a constant temperature T_b whose value changes as a parameter in the present computation. The cylinder surface is kept at a constant high temperature T_h.

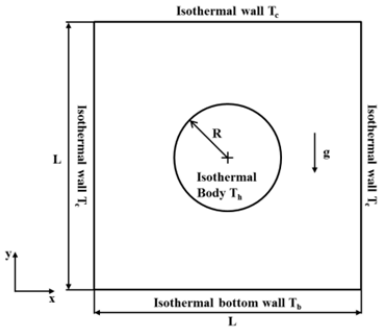

Figure 1 Computational domain and coordinate system along with boundary conditions

The governing equations describing steady incompressible viscous fluid flow and thermal fields are the continuity, momentum, and energy conservation equations in their non-dimensional forms, which are defined as

$$\frac{\partial u_i}{\partial x_i} - q = 0 \tag{1}$$

$$\frac{\partial u_i}{\partial t} + u_j \frac{\partial u_i}{\partial x_j} = -\frac{\partial P}{\partial x_i} + Pr \frac{\partial^2 u_i}{\partial x_j \partial x_j} + Ra\,Pr\,\theta\,\delta_{i2} + f_i \tag{2}$$

$$\frac{\partial \theta}{\partial t} + u_j \frac{\partial \theta}{\partial x_j} = \frac{\partial^2 \theta}{\partial x_j \partial x_j} + h \tag{3}$$

where the dimensionless variables in equations (1)-(3) are defined as follows:

$$t = \frac{t^* \alpha}{L^2},\ x_i = \frac{x_i^*}{L},\ u_i = \frac{u_i^* L}{\alpha},\ P = \frac{P^* L^2}{\rho \alpha^2},\ \theta = \frac{T^* - T_c^*}{T_h^* - T_c^*} \quad (4)$$

In equation (4), the superscript (*) denotes the dimensional variables; ρ and α represent the density and the thermal diffusivity of the fluid, respectively; P, θ, and t represent the dimensionless pressure, the dimensionless temperature, and the dimensionless time, respectively; x_i represents the dimensionless Cartesian coordinates; and u_i represents the corresponding dimensionless velocity components (where the subscripts i and j are the tensor notation with i =1, 2 and j =1, 2). Radiation effects were neglected and the fluid properties were assumed to be constant except in the buoyancy term according to the Boussinesq approximation. The aforementioned non-dimensionalization yielded two dimensionless parameters: $\mathrm{Pr} = \nu/\alpha$ and $Ra = \frac{g\beta L^3 (T_h - T_c)}{\nu\alpha}$, where ν, g, and β are the kinematic viscosity, gravitational acceleration, and volume expansion coefficient, respectively. The gravitational acceleration g acted in the negative y direction. The Prandtl number was set to $Pr = 0.7$, corresponding to the property of air. The Rayleigh number Ra varied in the range of $10^3 \sim 10^6$.

The immersed boundary method was used to represent the virtual surface of the inner circular cylinder with a no-slip boundary condition. The mass source/sink term q in equation (1) and the momentum forcing term f_i in equation (2) were applied on the body surface or inside the body to satisfy the no-slip condition and mass conservation in the cell containing the immersed boundary. In equation (3), heat source/sink h was applied to satisfy the isothermal boundary condition on the immersed boundary. The four-step time-split scheme was used to advance the flow field.

For the velocity field, no-slip and no-penetration boundary conditions were imposed on the walls. For the temperature fields, the hot dimensionless temperature of $\theta_h = 1$ was imposed on the wall of the inner cylinder, whereas the cold dimensionless temperature of $\theta_c = 0$ was imposed on the top and side walls of the enclosure. For the bottom wall of the enclosure, the dimensionless temperature varying in the range of $\theta_b = 0.0 \sim 1.0$ was imposed as an important variable to govern the fluid flow and heat transfer in the enclosure.

Once the velocity and temperature fields were obtained, the local and surface-averaged Nusselt numbers were calculated as follows:

$$Nu = \left.\frac{\partial \theta}{\partial n}\right|_{wall}, \quad \langle Nu \rangle = \frac{1}{S}\int_0^S Nu\, ds \quad (5)$$

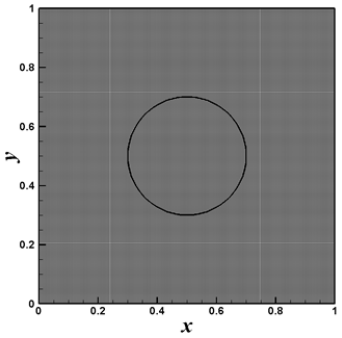

Figure 2 Distribution of the grid generated in the computational domain

Table 1 Grid dependency test results for the surface-averaged Nusselt number around the inner cylinder $\langle Nu_{cyl} \rangle$ when $Ra = 10^6$ and $\theta_b = 0.0$.

Grid number	$\langle Nu_{cyl} \rangle$	Difference (%)
202×202	4.9921	0.18
252×252	4.9902	0.21
302×302	4.9978	0.06
352×352	4.9998	0.02
402×402	5.0009	-

Table 2 Comparison of present surface-averaged Nusselt numbers at the hot inner cylinder with those of the previous numerical results

Ra	Surface-averaged Nusselt Number at the hot inner cylinder		Difference (%)
	Present study	Kim *et al.* [5]	
10^3	5.020	5.093	1.433
10^4	5.113	5.108	-0.098
10^5	7.750	7.767	-0.219
10^6	14.20	14.11	0.638

where n is the direction normal to the wall and S is the surface length. The uniform grid is distributed in the computational domain as shown in Figure 2. The numerical procedure is carried out the in-house code using FORTRAN scheme. Table 1 shows the grid dependency test results when $Ra = 10^6$ and $\theta_b = 0.0$. As shown in Table 1, the difference in the values of surface-averaged Nusselt number on the cylinder, $\langle Nu_{cyl} \rangle$, calculated using different grid points of 202×202, 252×252, 302×302, 352×352 and 402×402 for $Ra = 10^6$ and $\theta_b = 0.0$ is very small. Based on this grid

dependency test result, a grid resolution of 302×302 along horizontal (x) and vertical (y) directions was employed in the present study. To validate the present numerical methods, we compared the surface-averaged Nusselt number on the cylinder surface obtained from the present computation with that obtained by Kim *et al.* [5] obtained from their numerical simulation when $\theta_b = 0.0$, showing a good agreement between them with the maximum error less than 1.4%.

RESULTS AND DISCUSSION

Figure 3 shows the distribution of isotherms and streamlines in the enclosure for the case of $\theta_b = 0.0$ for different Rayleigh numbers of $Ra = 10^3$, 10^4, 10^5 and 10^6. The flow and thermal fields eventually reached the steady state for all simulation cases at four different Rayleigh numbers considered. In terms of general fluid motion occurring due to natural convection as shown in Figure 3, the heated lighter fluid is lifted along the hot surface of the inner cylinder due to buoyancy as a driving force. As the fluid flow approaches the cold top wall of the enclosure, it becomes gradually colder and denser. The fluid cools further as it moves along the cold top wall in the lateral direction. Finally, a denser fluid cooled moves downward along the cold side walls of the enclosure. Thus, the main circulation of the convection flow is formed in the enclosure.

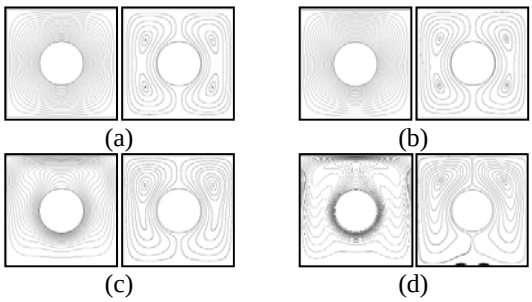

Figure 3 Isothermals (left) and streamlines (right) distributed in the enclosure; (a) $Ra = 10^3$, (b) $Ra = 10^4$, (c) $Ra = 10^5$ and (d) $Ra = 10^6$

When $Ra = 10^3$, the heat transfer in the enclosure mainly develops through a quasi-heat conduction process due to a very low convection velocity, as shown in the thermal fields of Figure 3(a). The main circulation flow in the enclosure shows a two-fold symmetric pattern about the vertical and horizontal center lines of the enclosure due to a very weak buoyancy effect that exhibits two inner vortices, as shown in Figure 3(a).

As we increase the Rayleigh number to $Ra = 10^5$, the role of convection in the heat transfer becomes more significant. As a result, the dominant convection flow occurs in the upper part of the cylinder where the thermal gradient is strong. The two inner vortices of each main circulation, which exists in the cases of $Ra = 10^3$ and $Ra = 10^4$, merge with each other at $Ra = 10^5$. Thus, a single vortex core of each main circulation is located in the upper part of the cylinder. At this Rayleigh number, a single upwelling plume can be clearly identified above the top surface of the cylinder, as shown in Figure 3(c). At $Ra = 10^6$, the heat transfer is mainly governed by the convection mode in the enclosure. Since the convection velocity significantly increases with increasing Rayleigh number, the boundary layer behavior can be clearly observed in regions of the lower part of cylinder and the upper part of the enclosure as shown in isotherms of Figure 3(d). The thermal boundary layer separates from the surface near the top of the cylinder and as a result a strong plume appears. As a result, the flow strongly impinges on the top of the enclosure, which also leads to form a thinner thermal boundary layer in this region and enhances the heat transfer. Tiny symmetric vortices appear in the vicinity of the bottom wall of the enclosure owing to the separation of the boundary layer by the strong convective flow.

Figure 4 shows the distribution of isotherms and streamlines at $Ra = 10^3$ according to the variation of θ_b. As shown in this figure, the variation in the bottom wall temperature has a small effect on the change in overall flow structures at the low Rayleigh number of $Ra = 10^3$. For the cases of $\theta_b = 0.1 \sim 1.0$, the twofold symmetric pattern in the main circulation is broken, unlike to that for the case of $\theta_b = 0.0$ shown in Figure 3(a). The main convection structure has a mirror symmetric pattern about the vertical center line of the enclosure, as shown in Figure 4(a)-(f). The sizes of inner vortices in the lower parts of the cylinder increases slightly, compared to those in the upper part of the cylinder because of the heating from the bottom wall of the enclosure. The isotherms in the lower part of the cylinder change their shape according to the variation of θ_b. As we increased θ_b at $Ra = 10^3$, the isotherms in the lower part of the cylinder increase in their values gradually as shown in Figure 4(a)-(f), resulting in a decrease in the thermal gradient near the lower surface of the cylinder. As we increase θ_b at $Ra = 10^3$, the isotherms gradually concentrate near each lower edge of the enclosure where the cold side and hot bottom walls are in contact. As a result, the thermal gradient around each lower edge of the enclosure becomes large.

Figure 5 shows the distribution of the local Nusselt number along the cylinder surface, the top wall of the enclosure and the bottom wall of the enclosure (Nu_{cyl}, Nu_t and Nu_b) at $Ra = 10^3$ for different values of θ_b. In this figure, the positive and negative values of the local Nusselt number are used to denote the direction of the heat transfer on the walls of the enclosure and cylinder surface. Positive values represent heat transfer from the surrounding fluid to the walls, and negative values represent the heat transfer from the walls to the surrounding fluid. When $\theta_b = 0.0$, Nu_{cyl} has a maximum value at $\varphi = 180^o$ which corresponds to the lower stagnation point in the cylinder and decreases slightly in its value with increasing φ from 180^o to $\varphi = 360^o$ (or decreasing φ from 180^o to $\varphi = 0^o$). The variation in the values of Nu_{cyl} according to φ at $\theta_b = 0.0$ is small in the absence of any heating from the bottom wall at the low Rayleigh number of $Ra = 10^3$, as shown in

Figure 5(a). However, when $\theta_b \geq 0.1$, because the fluid temperature in the lower part of the cylinder increases as a result of the heating from the bottom wall, the absolute values of Nu_{cyl} has a minimum value at $\varphi = 180^o$ and decrease with increasing θ_b. Especially, the change in the absolute values of Nu_{cyl} is large in the region of $\varphi = 90^o \sim 270^o$.

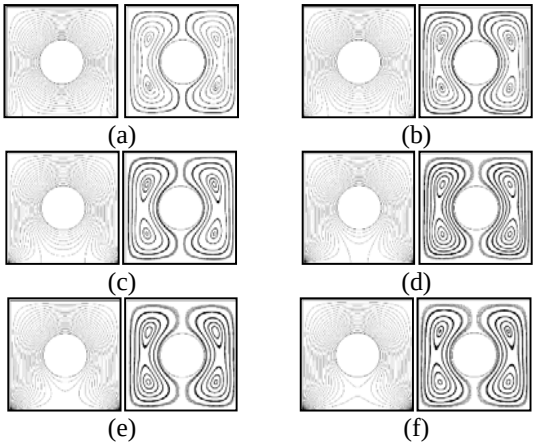

Figure 4 Isothermals (left) and streamlines (right) distributed in the enclosure at $Ra = 10^3$ (contour range from 0 to 1 with 21 levels); (a) $\theta_b = 0.2$, (b) $\theta_b = 0.4$, (c) $\theta_b = 0.6$, (d) $\theta_b = 0.8$, (e) $\theta_b = 0.9$ and (f) $\theta_b = 1.0$

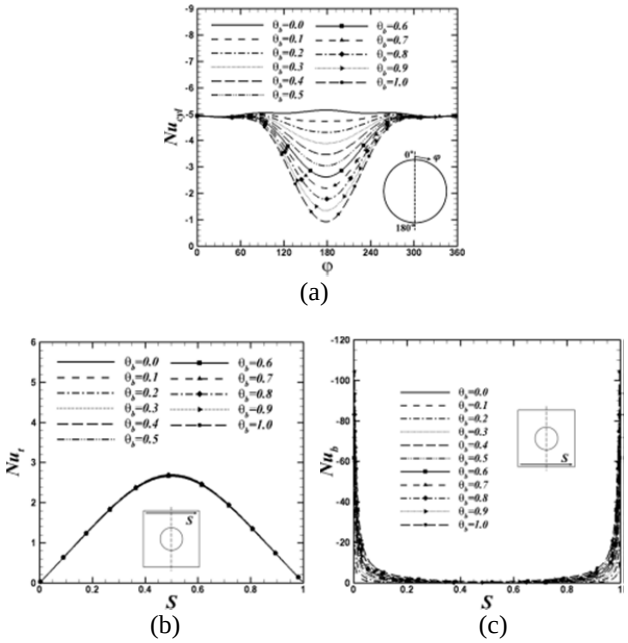

Figure 5 Distribution of the local Nusselt number along the cylinder surface, the top wall of the enclosure and the bottom wall of the enclosure (Nu_{cyl}, Nu_t and Nu_b) at $Ra = 10^3$ for different values of θ_b

As shown in Figure 5(b), the distribution of Nu_t does not depend on θ_b under the dominant conduction heat transfer mode at the low Rayleigh number of $Ra = 10^3$. For all cases of $\theta_b = 0.0 \sim 1.0$ considered, Nu_t has the maximum value at the center of the top wall ($S = 0.5$) because the distance between the cold top wall and hot cylinder surface has the smallest value. As shown in Figure 5(c), Nu_b has the highest value around each lower corner of the enclosure at $S = 0.0$ and $S = 1.0$ due to a large temperature difference between the side walls and the bottom wall of the enclosure.

Figure 6 shows the distribution of isotherms and streamlines at $Ra = 10^5$ according to the variation of θ_b. When $\theta_b = 0.4$ in Figure 6(b), small inner vortices start to be formed in the lower part of the cylinder because of the increase in the thermal gradient in the lower part of the cylinder, which is caused by the increase in temperature of the bottom wall. As we increase θ_b from 0.4 to 0.8, the thermal gradient between the bottom wall and the cylinder surface becomes continuously stronger; thus, the inner vortices in the lower part of the cylinder gradually increase in size. By following the circulation flow of the lower inner vortices, the isotherms are distorted further as θ_b increases.

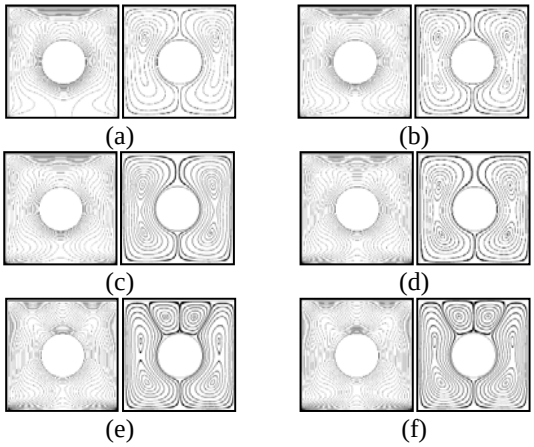

Figure 6 Isothermals (left) and streamlines (right) distributed in the enclosure at $Ra = 10^5$ (contour range from 0 to 1 with 21 levels); (a) $\theta_b = 0.2$, (b) $\theta_b = 0.4$, (c) $\theta_b = 0.6$, (d) $\theta_b = 0.8$, (e) $\theta_b = 0.9$ and (f) $\theta_b = 1.0$

When $\theta_b = 0.9$, a pair of secondary vortices form and separate from the main circulation flow above the top surface of the cylinder as shown in Figure 6(e). This pair rotates in the clockwise and counter clockwise directions. The upwelling flow, which is induced by a strong buoyancy effect, occurs around the locations of $\varphi = 60^o$ and $\varphi = 270^o$ on the surface of cylinder. In addition, the descending flow from the top wall to the cylinder surface is generated above the top surface of the cylinder along the vertical centerline of the enclosure because of the presence of the secondary vortices. The upper part of the

main circulation is confined around the side wall of the enclosure. As a result, the inner vortices distributed in the upper part of the cylinder shrink in size, and the vortex cores move downward. As shown in the temperature field in Figure 6(e), a single upwelling plume at $\theta_b = 0.2 \sim 0.8$ is divided into a pair of upwelling plumes at $\theta_b = 0.9$. The plumes are formed near $\varphi = 60^o$ and $\varphi = 270^o$ on the cylinder surface by following the upwelling flow separating from the cylinder surface. The isotherms are sparser near the surface of cylinder but denser near the top wall due to the presence of the pair of upwelling plumes, while the isotherms are denser near the cylinder surface but sparser near the top wall due to the presence of the descending flow of secondary vortices. The overall flow and thermal structures at $\theta_b = 1.0$ are very similar to those at $\theta_b = 0.9$.

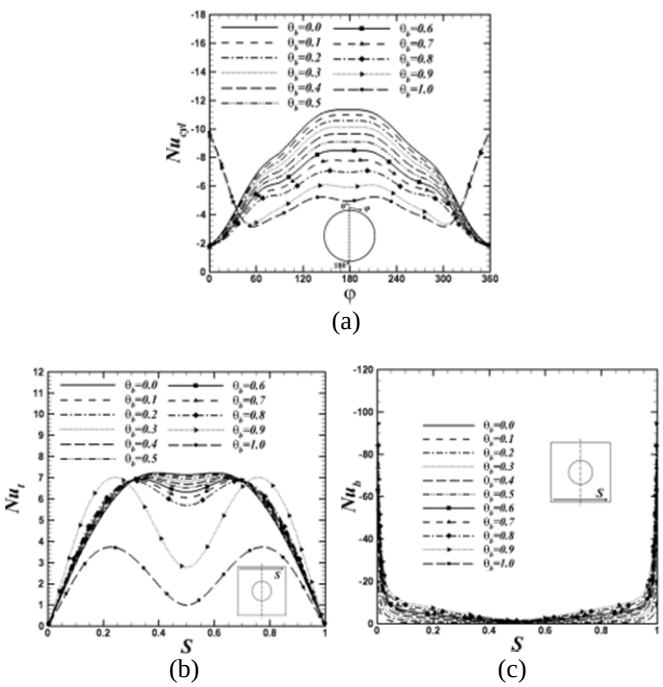

Figure 7 Distribution of the local Nusselt number along the cylinder surface, the top wall of the enclosure and the bottom wall of the enclosure (Nu_{cyl}, Nu_t and Nu_b) at $Ra = 10^5$ for different values of θ_b

Figure 7 shows the distribution of the local Nusselt number along the cylinder surface, the top wall of the enclosure and the bottom wall of the enclosure (Nu_{cyl}, Nu_t and Nu_b) at $Ra = 10^5$ for different values of θ_b. The distribution shapes of Nu_{cyl} and Nu_t at $Ra = 10^5$ are different from that at $Ra = 10^3$ and 10^4 because the distribution of the fluid flow and isotherms at $Ra = 10^5$ is much different from that at $Ra = 10^3$ and 10^4. As shown in Figure 7(a), the minimum absolute value of Nu_{cyl} occurs at $\varphi = 0^o$ (or $\varphi = 360^o$) for the cases of $\theta_b = 0.0 \sim 0.8$ because of the presence of a single upwelling plume. For the cases of $\theta_b = 0.0 \sim 0.8$, the absolute value of Nu_{cyl} monotonically increases with increasing φ from $\varphi = 0^o$ to $\varphi = 180^o$, and Nu_{cyl} has the maximum absolute value at $\varphi = 180^o$. However, for the cases of $\theta_b = 0.9$ and 1.0, Nu_{cyl} has the maximum absolute value at $\varphi = 0^o$ (or $\varphi = 360^o$) because of the descending flow of the secondary vortices that forms above the top surface of the cylinder, unlike the cases of $\theta_b = 0.0 \sim 0.8$. Nu_{cyl} has the minimum absolute values at $\varphi = 60^o$ and $\varphi = 300^o$ because of the presence of a pair of the upwelling plumes. For all cases of $\theta_b = 0.0 \sim 1.0$, the absolute values of Nu_{cyl} gradually increase with increasing θ_b, except for $\varphi = 0^o \sim 60^o$ and $\varphi = 300^o \sim 360^o$ at $\theta_b = 0.9$ and 1.0. As shown in Figure 7(b), the distribution of Nu_t has high two peaks on the top wall of the enclosure for all cases of $\theta_b = 0.0 \sim 1.0$. For the cases of $\theta_b = 0.0 \sim 0.8$, which have a single upwelling plume above the top surface of the cylinder, the two high peaks occur around the center region of the top wall at $S = 0.35 \sim 0.65$ depending on the value of θ_b. As shown in Figure 7(c), the distribution shapes of Nu_b according to S on the bottom wall at $Ra = 10^5$ are similar to those at $Ra = 10^3$ shown in Figure 5(c). However, the variation of Nu_b according to θ_b at $Ra = 10^5$ is relatively larger than that at $Ra = 10^3$ around the side walls since the cold fluid is further encouraged into the lower part of the cylinder by the strengthened convection flow with increasing Rayleigh number.

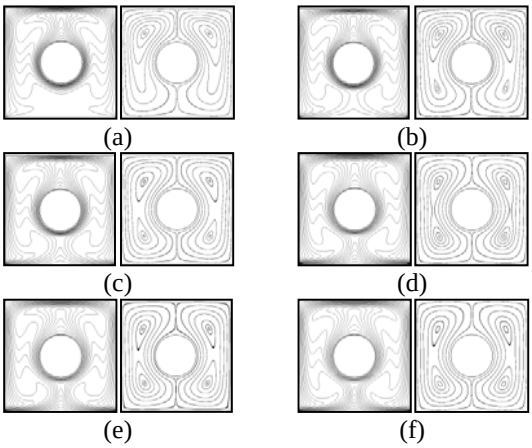

Figure 8 Isothermals (left) and streamlines (right) distributed in the enclosure at $Ra = 10^6$ (contour range from 0 to 1 with 21 levels); (a) $\theta_b = 0.2$, (b) $\theta_b = 0.4$, (c) $\theta_b = 0.6$, (d) $\theta_b = 0.8$, (e) $\theta_b = 0.9$ and (f) $\theta_b = 1.0$

Figure 8 shows the distribution of isotherms and streamlines at $Ra = 10^6$ according to the variation of θ_b. When $Ra = 10^6$, the magnitude of convection velocity becomes much larger

than that when $Ra = 10^5$. As a result, when $Ra = 10^6$, much stronger rising plumes than those for $Ra = 10^5$ are formed on the top of the cylinder. Because of the effects of the strong convection and rising thermal plume impinging on the top surface of the enclosure at $Ra = 10^6$, thinner thermal boundary layers are formed on the surfaces of the cylinder and the top surfaces of the enclosure, resulting in a much larger heat transfer rate than at $Ra = 10^5$.

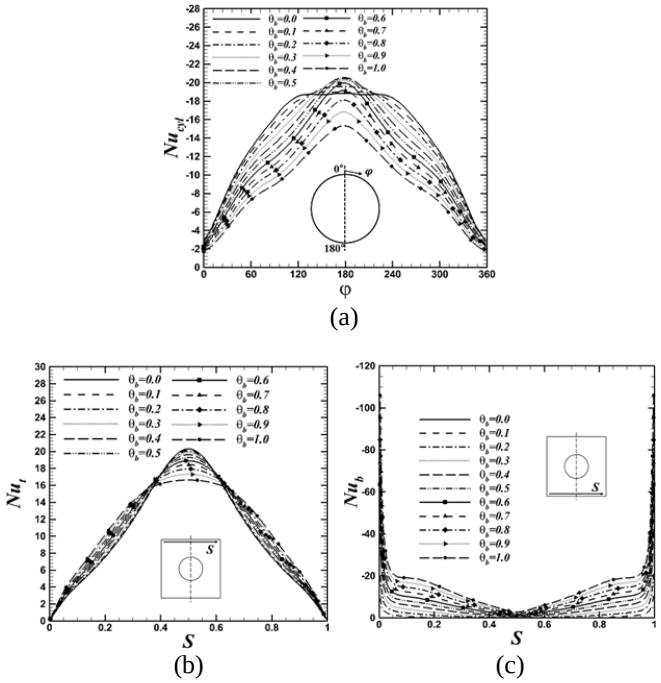

Figure 9 Distribution of the local Nusselt number along the cylinder surface, the top wall of the enclosure and the bottom wall of the enclosure (Nu_{cyl}, Nu_t and Nu_b) at $Ra = 10^6$ for different values of θ_b

Figure 9 shows the distribution of the local Nusselt number along the cylinder surface, the top wall of the enclosure and the bottom wall of the enclosure (Nu_{cyl}, Nu_t and Nu_b) at $Ra = 10^6$ for different values of θ_b. Because the effect of convection on the heat transfer in the enclosure becomes much larger with increasing Rayleigh number, the absolute values of the local Nusselt numbers at $Ra = 10^6$ are much larger than those at $Ra = 10^3$, 10^4 and 10^5. As a result, the distribution of local Nusselt numbers at $Ra = 10^6$ is also different from that at $Ra = 10^5$. When $\theta_b = 0.0$, the absolute value of Nu_{cyl} has the almost uniform maximum value around $\varphi = 120^o \sim 240^o$ which corresponds to the lower surface of the cylinder including the lower stagnation point of the cylinder. When we increase θ_b, the region at which the absolute value of Nu_{cyl} has an almost constant value at the lower surface of the cylinder becomes narrower because of the added effect of heating from the hot cylinder and the bottom wall. As a result, when $\theta_b \geq 0.3$, the absolute value of Nu_{cyl} has the maximum peak value at $\varphi = 180^o$, resulting in monotonically decreasing absolute value of Nu_{cyl} with decreasing (or increasing) φ from $\varphi = 180^o$ to $\varphi = 0^o$ (or $\varphi = 360^o$) because of the thermal boundary layer development along the cylinder surface. When $0 \leq \theta_b \leq 0.3$, the maximum absolute value of Nu_{cyl} at $\varphi = 180^o$ increases with increasing θ_b due to the added effect of heating from the hot cylinder and the bottom wall on the rising thermal plume along the cylinder surface. However, as we increase θ_b at $0.3 \leq \theta_b \leq 1.0$, the maximum absolute value of Nu_{cyl} at $\varphi = 180^o$ decreases because the temperature difference between the hot cylinder and the bottom wall decreases and as a result the thermal gradient around the lower stagnation point of the cylinder decreases. When $\theta_b = 0.9$ and 1.0 at $Ra = 10^5$, Nu_{cyl} has the maximum absolute value at $\varphi = 0^o$ and $\varphi = 360^o$ while it has the minimum absolute values at $\varphi = 60^o$ and $\varphi = 300^o$, because of the presence of a pair of the upwelling plumes formed on the top surface of the cylinder. However, when $\theta_b = 0.9$ and 1.0 at $Ra = 10^6$, a pair of the upwelling plumes are not formed on the top surface of the cylinder and the distribution of streamlines and isotherms is similar to that when $0.3 \leq \theta_b \leq 0.8$ at $Ra = 10^6$, as shown in Figure 8(a)-(f). As a result, when $\theta_b = 0.9$ and 1.0 at $Ra = 10^6$, Nu_{cyl} has the minimum absolute value at $\varphi = 0^o$ (or $\varphi = 360^o$), while it has the maximum absolute values at $\varphi = 180^o$, similar to that when $0.3 \leq \theta_b \leq 0.8$ at $Ra = 10^6$ but unlike to that when $\theta_b = 0.9$ and 1.0 at $Ra = 10^5$. As shown in Figure 9(b), the distribution of Nu_t at $Ra = 10^6$ has the maximum one peak at the center of the top wall of the enclosure ($S = 0.5$) for all cases of $\theta_b = 0.0 \sim 1.0$, compared to two high peaks and one low peak of Nu_t at $Ra = 10^5$ as shown in Figure 7(b), because the strength of the thermal plume rising from the cylinder upper surface becomes much larger with increasing Rayleigh number from $Ra = 10^5$ to $Ra = 10^6$. The distribution shapes of Nu_b according to S on the bottom wall at $Ra = 10^6$ are similar to those at $Ra = 10^3$, 10^4 and 10^5, which has the maximum value at the side walls ($S = 0.0$ and 1.0) and the minimum values close to zero at the center of the bottom wall ($S = 0.5$), as shown in Figure 5(c), Figure 7(c) and Figure 9(c). Similarly, the absolute value of Nu_b is almost zero at $\theta_b = 0.0$ because of the formation of the large stagnation region between the lower surface of the cylinder and the bottom wall at the high Rayleigh number of 10^6, as shown in Figure 3(d).

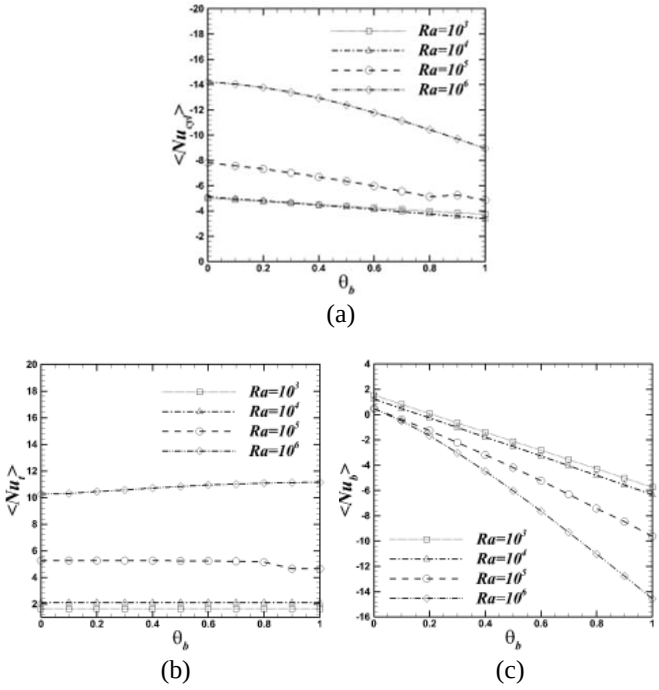

Figure 10 Distributions of the surface-averaged Nusselt number as a function of θ_b for four different Rayleigh numbers; (a) cylinder surface, (b) top wall and (c) bottom wall

Figure 10 shows the distributions of the surface-averaged Nusselt number on the cylinder surface, top wall, and bottom wall of the enclosure ($\langle Nu_{cyl} \rangle$, $\langle Nu_t \rangle$, and $\langle Nu_b \rangle$, respectively) as a function of θ_b for three different Rayleigh numbers considered in our study. In these figures, as previously mentioned, positive or negative values of the Nusselt number denote the direction of the heat transfer on the walls.

As shown in Figure 10(a), the absolute value of $\langle Nu_{cyl} \rangle$ decreases monotonically with increasing θ_b at $Ra = 10^3$ and $Ra = 10^4$ since the fluid temperature around the cylinder gradually increases with increasing θ_b . The absolute values at $Ra = 10^4$ are slightly augmented for the cases of $\theta_b = 0.0 \sim 0.3$ and are slightly reduced for the cases of $\theta_b = 0.4 \sim 1.0$, compared to the cases of $Ra = 10^3$. When $Ra = 10^5$, the absolute value of $\langle Nu_{cyl} \rangle$, having a decreasing trend from $\theta_b = 0.0$ to $\theta_b = 0.8$, slightly increases at $\theta_b = 0.9$ because of the effect of the descending flow of the secondary vortices that are formed above the top surface of the cylinder, as shown in Figure 6(e). As we increase θ_b from $\theta_b = 0.9$ to $\theta_b = 1.0$, the absolute value of $\langle Nu_{cyl} \rangle$ decreases again. When $Ra = 10^6$, the absolute values of $\langle Nu_{cyl} \rangle$ increases further compared to the cases of $Ra = 10^3$, $Ra = 10^4$ and $Ra = 10^5$. As a result, the temperature difference between the hot cylinder surface and the surrounding fluid decreases sharply as θ_b increases, which results in a rapid decrease in heat transfer on the cylinder surface with increasing θ_b . As shown in Figure 10(b), the variation of $\langle Nu_t \rangle$ according to θ_b is very small for $Ra = 10^3$ and $Ra = 10^4$. For $Ra = 10^5$ with higher values of $\langle Nu_t \rangle$ than those for the cases of $Ra = 10^3$ and $Ra = 10^4$, the value of $\langle Nu_t \rangle$ slightly decreases with increasing θ_b from 0.0 to 0.8. When $\theta_b = 0.9$ at $Ra = 10^5$, the value of $\langle Nu_t \rangle$ steeply decreases because of the influence of a pair of secondary vortices that is formed above the top surface of the cylinder. At $Ra = 10^6$, as θ_b increases, $\langle Nu_t \rangle$ increases because of an increase in the heat transfer capacity around the center of the top wall, as shown in Figure 9(a).

CONCLUSIONS

Two-dimensional numerical simulations were performed for natural convection in a square enclosure with an hot inner cylinder for four different Rayleigh numbers of 10^3 , 10^4 , 10^5 and 10^6 , by using the immersed boundary method to provide an in-depth analysis of various phenomena associated with natural convection such as the formation of the vortex structure and the corresponding heat transfer based on the various temperature conditions of bottom wall.

When $Ra = 10^3$ and $Ra = 10^4$, variations in the value of the bottom temperature have little effect on thermal and flow structures, although there are small variations in the convection velocity in the enclosure. Consequently, there is a little difference in the overall heat transfer capacity in terms of the Nusselt number between the top wall and the cylinder surface based on variations θ_b . A primary vortex pair showing a mirror symmetric pattern at $Ra = 10^3$ and $Ra = 10^4$. For the cases of $Ra = 10^3$, the temperature variation of the bottom wall had little influence on the change in overall flow structures. In the cases of $\theta_b = 0.1 \sim 1.0$, the two-fold symmetric pattern of the main circulation at $\theta_b = 0.0$ was slightly broken, and the main convection structure with a mirror-symmetric pattern about the vertical centerline of the enclosure was distributed in the enclosure. The sizes of inner vortices in the lower parts of the cylinder became slightly larger than those in the upper part of the cylinder. For the cases of $Ra = 10^4$, the main convection structures show a mirror symmetric pattern about the vertical centerline of the enclosure for all cases of $\theta_b = 0.0 \sim 1.0$. With increasing θ_b , the inner vortices in the lower part of the cylinder gradually increased in size.

For the cases of $Ra = 10^5$, the small inner vortices of the cylinder started to form in the lower part of the cylinder at $\theta_b = 0.2$ with increasing θ_b . Then, the lower inner vortices gradually increased in size with increasing θ_b to $\theta_b = 0.8$. For the cases of $\theta_b = 0.9 \sim 1.0$, a pair of secondary vortices separating from the main convection structure formed above

the top surface of the cylinder because of the strong buoyancy effect.

For the cases of $Ra = 10^6$, the small inner vortices of the cylinder started to form in the lower part of the cylinder at $\theta_b = 0.4$ with increasing θ_b which is caused by the increase in temperature of the bottom wall. For the cases of $\theta_b = 0.4 \sim 1.0$, the thermal gradient becomes continuously stronger; thus, the inner vortices in the lower part of the cylinder gradually increase in size. By following the circulation flow of the lower inner vortices, the isotherms are more distorted further as θ_b increases compared to $Ra = 10^5$. The generation and dissolution of vortices are dependent mainly on the temperature of bottom wall in the enclosure.

REFERENCES

[1] A. Y. Gelfgat, Different modes of Rayleigh–Bénard instability in two- and three-dimensional rectangular enclosures, *Journal of Computational Physics*, Vol. 156, 1999, pp. 300-324

[2] N. Quertatani, N. B. Cheikh, B. B. Beya and T. Lili, Numerical simulation of two-dimensional Rayleigh–Bénard convection in an enclosure, *Comptes Rendus Mecanique*, Vol.336, 2008, pp. 464-470

[3] M. C. D'Orazio, C. Cianfrini and M. Corcione, Rayleigh–Bénard convection in tall rectangular enclosures, *International Journal of Thermal Science*, Vol. 43, 2004, pp. 135-144

[4] M. Corcione, Effects of the thermal boundary conditions at the sidewalls upon natural convection in rectangular enclosures heated from below and cooled from above, *International Journal of Thermal Science*, Vol. 42, 2003, pp. 199-208

[5] B.S. Kim, D.S. Lee, M.Y. Ha and H.S. Yoon, A numerical study of natural convection in a square enclosure with a circular cylinder at different vertical locations, *International Journal of Heat and Mass Transfer*, Vol. 51, 2008, pp. 1888-1906

[6] P. Kandaswamy, N. Nithyadevi and C. O. Ng, Natural convection in enclosures with partially thermally active side walls containing internal heat sources, *Physics of Fluids*, Vol. 20 (9), 2008, pp. 097104-1-9

[7] O. Aydin and W. Yang, Natural convection in enclosures with localized heating from below and symmetrical cooling from sides, *International Journal of Numerical Methods for Heat and Fluid Flow*, Vol. 10 (5), 2000, pp. 518-529

[8] T. Basak, S. Roy and A. R. Balakrishnan, Effect of thermal boundary condition on natural convection flows within a square cavity, *International Journal of Heat and Mass Transfer*, Vol. 49, 2006, pp. 4525-4535

[9] M.Y. Ha, I.K. Kim, H.S. Yoon, K.S. Yoon, J.R. Lee, S. Balachandar and H.H. Chun, Two-dimensional and unsteady natural convection in a horizontal enclosure with a square body, *Numerical Heat Transfer Part A*, Vol. 41, 2002, pp. 183-210

[10] J.R. Lee, M.Y. Ha, S. Balachandar, H.S. Yoon and S.S. Lee, Natural convection in a horizontal layer of fluid with a periodic array of square cylinders in the interior, *Physics of Fluids*, Vol. 16 (4), 2004, pp. 1097-1117

[11] J. Kim and P. Moin, Application of a fractional step method to incompressible Navier–Stokes equations, *Journal of Computational Physics*, Vol. 59, 1985, pp. 308-323.

[12] J. Kim, D. Kim, H. Choi, An immersed-boundary finite volume method for simulations of flow in complex geometries, *Journal of Computational Physics*, Vol.171, 2001, pp. 132-150